Original Research

Fully Automatic Segmentation of the Brain From T1-Weighted MRI Using *Bridge Burner* Algorithm

Artem Mikheev, MS, Gregory Nevsky, MD, Siddharth Govindan, MD, Robert Grossman, MD, and Henry Rusinek, PhD*

Purpose: To validate *Bridge Burner*, a new brain segmentation algorithm based on thresholding, connectivity, surface detection, and a new operator of constrained growing.

Materials and Methods: T1-weighted MR images were selected at random from three previous neuroimaging studies to represent a spectrum of system manufacturers, pulse sequences, subject ages, genders, and neurological conditions. The ground truth consisted of brain masks generated manually by a consensus of expert observers. All cases were segmented using a common set of parameters.

Results: *Bridge Burner* segmentation errors were 3.4% ± 1.3% (volume mismatch) and 0.34 ± 0.17 mm (surface mismatch). The disagreement among experts was 3.8% ± 2.0% (volume mismatch) and 0.48 ± 0.49 mm (surface mismatch). The error obtained using the brain extraction tool (BET), a widely used brain segmentation program, was 8.3% ± 9.1%. *Bridge Burner* brain masks are visually similar to the masks generated by human experts. Areas affected by signal intensity nonuniformity artifacts were occasionally undersegmented, and meninges and large sinuses were often falsely classified as the brain tissue. Segmentation of one MRI dataset takes seven seconds.

Conclusion: The new fully automatic algorithm appears to provide accurate brain segmentation from high-resolution T1-weighted MR images.

Key Words: image analysis; segmentation; brain; morphometry; magnetic resonance imaging (MRI); neuroimaging
J. Magn. Reson. Imaging 2008;27:1235–1241.
© 2008 Wiley-Liss, Inc.

SEGMENTATION OF THE BRAIN is an important preprocessing step in neuroimaging applications. Total brain volumes and subsequent brain atrophy estimation in patients suffering from various pathologies, including traumatic injury, multiple sclerosis, or dementia, are useful estimates of brain injury and its response to treatment (1,2). Brain segmentation is the initial step in studies of the global and regional brain shape and volume (3–7). These studies are taking place with increasing frequency in research on normal brain development during childhood, normal aging, and neurological and psychiatric disorders. Coregistration of functional brain data with high-resolution MR or computed tomography (CT) images is another area that benefits from brain segmentation (8,9). There is little nonbrain tissue signal in functional imaging such as positron emission tomography (PET), single-photon emission CT (SPECT), or functional MRI (fMRI), whereas structural MR images may contain high signal intensity from nonbrain tissue. As a result, most multimodality registration algorithms work best when processing of structural data is restricted to brain voxels. Segmentation of the brain is also a key step in cortical surface modeling and visualization.

The tedious and expensive nature of manual outlining of the brain provided the impetus for the development of several automated and semiautomated skull-stripping systems. Several sophisticated algorithms have been developed and extensively tested in recent publications (10–14). These programs have greatly reduced the amount of time needed to segment brain tissue compared to manual extraction. However, the majority of algorithms include ventricular and subarachnoid cerebrospinal fluid (CSF) in the resulting brain mask, which limits their direct application to studies of neuronal loss and to brain surface rendering and visualization. Moreover, current tools force the user to compromise either processing speed or accuracy.

We have developed and tested *Bridge Burner*, an algorithm that appears to combine fast computational performance with high segmentation accuracy when applied to current high-resolution three-dimensional (3D) T1-weighted MRI. The algorithm exploits the notion that the brain and nonbrain structures are either: 1) not connected to one another; 2) connected by a set of voxels (a Bridge) that is "thin" relative to the brain gyri (Fig. 1); or 3) separated by a strong edge.

The accuracy and the processing time of *Bridge Burner* are compared to manual segmentation (consen-
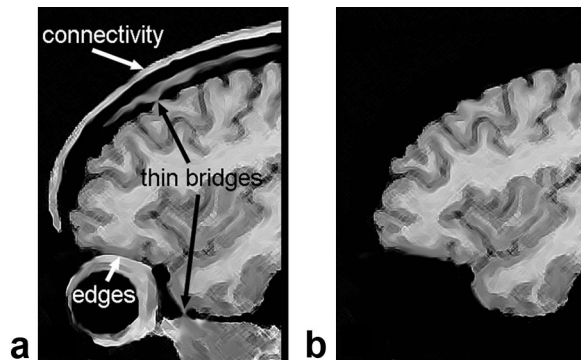
Figure 1. *Bridge Burner* uses thresholding, connectivity, edge detection, and a novel morphological operator of constrained growing to extract dominant features (**b**) from a 3D image (**a**).

sus of human experts) and to the brain extraction tool (BET), a popular fully-automatic brain segmentation tool (10). The T1-weighted MR images used in this validation study spanned a range of ages, brain disorders, and acquisition protocols.

MATERIALS AND METHODS

Segmentation Algorithm

The algorithm begins by estimating the signal intensity of the cerebral white matter, S_w. This is done by searching a 1-cm thick midcoronal slab of the head for a $1 \times 1 \times 1$ cm^3 cube that maximizes the ratio of the average value of signal intensity to its standard deviation (Fig. 2a). The resulting sample of pure white matter signal S_w is used for the initial segmentation based on intensity thresholding, generating the set V_0 of voxels

$$V_0 = \{v : S_w t_{min} < I(v) < S_w t_{max}\}, \qquad [1]$$

where $I(v)$ is the signal intensity of voxel v and t_{min} and t_{max} are dimensionless parameters determined relative to S_w. The aim is to include within V_0 the entire cerebral gray and white matter, while excluding the CSF, fat, and air (Fig. 2a). Some nonbrain soft tissue such as muscle, blood vessels, and voxels that contain a partial volume of fatty tissue will be included in V_0.

A 3D edge detector (15) is then invoked to generate the set E of voxels (Fig. 2b) at which the magnitude of Canny 3D edges $G(v)$ exceeds a threshold,

$$E = \{v : |G(v)| > S_w t_{grad}\}, \qquad [2]$$

where the edge threshold parameter t_{grad} is also normalized to the white matter signal S_w. The resulting set is combined with the set S_0 of surface voxels of V_0 to form the boundary set S:

$$S = S_0 \cup (E \cap V_0). \qquad [3]$$

(A voxel is defined to be on the surface of A if $v \in A$ and v is adjacent to a voxel not in A.)

The goal of the next step is to identify the "peel layer" of V_0. Originating with voxels v_1 in the boundary set S, the program considers paths

$$\{v_1 \in S, v_2 \in V_0 \cap adj(v_1), \ldots, v_n \in V_0 \cap adj(v_{n-1})\}, \quad [4]$$

where adj(v) is the set of all 26 neighbors of v. There are three possible values of the distance between adjacent voxels: 1, $\sqrt{2}$, and $\sqrt{3}$. The length of a path is the sum of the Euclidean distances between consecutive voxels within the path:

$$\sum_{i=1}^{n-1} |v_i, v_{i+1}|. \qquad [5]$$

The peel layer P consists of all paths of length less than p, which is the fourth parameter of the algorithm. A set of interior voxels V_1 is next constructed as $V_1 = V_0 - P$, i.e., by deleting the peel layer from V_0 (Fig. 2c). For optimal segmentation, p must exceed the "width" of all bridges that connect the brain with nonbrain tissue.

The set V_1 consists of several connected components. The largest component, V_C (Fig. 2d), will ideally exclude nonbrain tissue.

We then apply the growth operation that aims to enlarge the set V_C until it reaches the brain surface (Fig. 2e). This is done by considering constrained paths

$$\{w_1 \in surf(V_C), w_2 \in P \cap \hat{S} \cap adj(w_1),$$
$$\ldots, w_n \in P \cap \hat{S} \cap adj(v_{n-1})\} \quad [6]$$

where $surf(V_C)$ denotes the set of surface voxels of V_C and $\hat{S}$ is the complement of the boundary set S defined in Eq. [3]. In other words, the path originates at a surface of V_C, extends through the peel layer P, but is
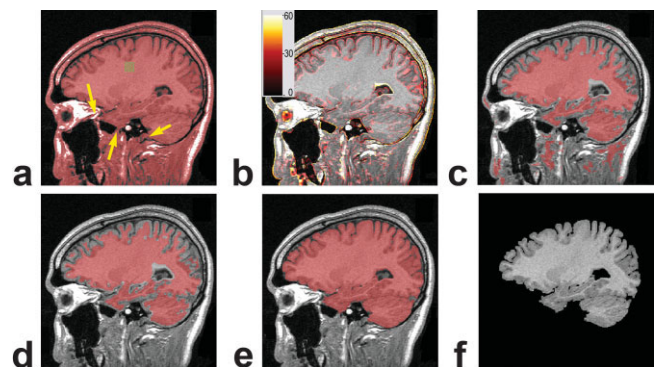
Figure 2. a: The white matter sample (green box) is constructed by searching the midcoronal slab for a 1-cm^3 cube with a high and homogeneous signal. Initial segmentation V_0, (in red) is superimposed on a T1-weighted image. The arrows indicate the locations of bridges, i.e., thin connections between the brain and nonbrain tissue. **b:** Edge voxels (hot color map) superimposed on the image. **c:** The interior set V_1 (in red) is obtained by peeling a layer of thickness $p = 2.7$ voxels from the boundary of the initial set V_0 shown in (b). **d:** The largest connected component of the interior set. **e:** Final brain mask superimposed on the image. **f:** Segmented brain.

not allowed to intersect the set **S**. The growth layer **G** is constructed as the set of such paths of length less than *g*, the last parameter of the algorithm. The five parameters of *Bridge Burner* are t_{min}, t_{max}, t_{grad}, p, and g. The final brain mask (Fig. 2e) is the union of V_C with **G**. To segment the brain, all voxels outside the mask are set to zero intensity (Fig. 2f).

Bridge Burner is implemented using the Visual Sudio C++ compiler (Microsoft Corp., Redmond, WA, USA) for the Microsoft Windows operating system.

Test Images

For testing and validation we have assembled T1-weighted images that represent a spectrum of system manufacturers, pulse sequences, and ages, genders, and neurological conditions of subjects. These 1.5-T images were selected at random from three much larger research databases of scans at our institution.

AD Set

A total of 10 data sets were obtained with GE Signa (General Electric, Milwaukee, WI, USA) using the gradient recalled echo (GRE) sequence with parameters: TR = 35 msec, TE = 9 msec, flip angle (FA) = 60°, in either coronal or axial orientation. Coronal slices were 1.3-mm thick; field of view (FOV) = 180 × 180 × 165 mm, and acquisition matrix size = 256 × 192 × 124. Axial slices were 1.5-mm thick, FOV = 240 × 240 × 186 mm, and acquisition matrix size = 256 × 192 × 124. The subjects were five elderly normal volunteers and five patients diagnosed with probable Alzheimer's Disease, four men and six women, 66–83 years old.

SZ Set

A total of eight data sets were acquired on Picker Vista HPQ system (Picker International, Cleveland, OH, USA) using the GRE sequence with parameters: TR = 33 msec, TE = 11 msec, FA = 35°, coronal slices 2.8-mm thick; FOV = 240 × 240 × 240 mm, acquisition matrix size = 256 × 256 × 85. The subjects were four healthy volunteers and four schizophrenic patients, all male, 27–53 years old.

BI Set

A total of eight data sets were acquired on Siemens Vision (Siemens Medical Systems, Erlangen, Germany) using the magnetization prepared rapid gradient echo (MPRAGE) sequence: TR = 9.7 msec, TE = 4 msec, TI = 1000 msec, FA = 15°, sagittal slices 1.5-mm thick, FOV = 210 × 210 × 192 mm, acquisition matrix size = 256 × 256 × 128. The subjects were four healthy volunteers and four patients with brain trauma (no open injury), four men and four women, 18–42 years old.

HR Set

A total of three 3D sets were used to test the ability of the system to process high-resolution 512 × 512 images. One set was acquired on Siemens Avanto (MPRAGE, 175 × 0.7-mm coronal slices) and two on GE Signa using the GRE sequence: one had 165 axial slices, and the other 160 sagittal slices, both were 1-mm-thick and had an FOV = 250 × 250 mm.

Scan-Rescan Set

To test the precision of measuring brain volume over time, we analyzed multiple MRIs on five healthy, 59–72 years old volunteers. Each person was imaged four times using the same (sagittal MPRAGE 256 × 256) protocol. Imaging was done at two sessions separated by one to six months. A total of two 3D datasets were acquired at each session without moving the person out of the magnet.

Manual Segmentation by Human Experts

To provide the ground truth, brain masks were generated manually by a team of seven observers (one radiologist, one neuroimaging researcher, two medical residents in radiology, and three medical students) who had one to 14 years of experience in neuroanatomy and neuroradiology. Observers used an interactive image analysis software package (16) to generate brain masks. The following tools and their combinations were used: a mouse-controlled "paintbrush," an "eraser," an electronic pencil to trace the edges, and a "threshold" tool to separate tissues with different signal intensities. The CSF was excluded from the brain mask. Observers were randomly assigned to cases, resulting in three independent segmentations of each scan. All observers were encouraged to consult the brain atlas (17). Those less experienced with MRI were instructed on how sinuses and dura matter are depicted on T1-weighted images. Since manual segmentation of one complete brain (averaging about 100 sections) requires approximately six hours, one-fifth of each volume (slices with numbers that are a multiple of 5) were traced. Individual masks were combined into the ground truth consensus mask using the simultaneous truth and performance level estimation (STAPLE) algorithm (18). Since the 5 × 4 scan-rescan images served to verify the consistency of automatic brain volume measurement, these images were not segmented manually.

Segmentation Using the BET

For comparison, each case was segmented using the BET, a fully automated, and freely available program (10). BET begins by estimating the threshold between the brain and CSF, then it determines the center of gravity C of the head, constructs a small tessellated surface F (initially a sphere) centered at C, and it incrementally adjusts the vertices of F to balance its smoothness and the desired signal intensity criteria. The main parameter of the BET algorithm is the "preset constant" b_t (see Eq. [11] in Ref. 10), with the default value of 0.5. To compare BET output with *Bridge Burner* and our ground truth masks, we had to eliminate from BET all CSF voxels. This was done by deleting voxels with intensity below $t_{CSF} \, S_w$, where S_w is the white matter signal defined in the Segmentation Algorithm section. The two parameters of BET were therefore b_t, and t_{CSF}.

Table 1
Optimization of *Bridge Burner* Parameters*

Group	t_{min}	t_{max}	t_{grad}	p	g	E_{opt} (%)	E_{med} (%)
AD	0.54	1.39	0.36	2.4	6.7	1.84	1.87
SZ	0.53	1.35	0.32	2.8	6.4	2.52	2.56
BI	0.51	1.30	0.43	2.7	5.1	2.80	2.83
Median	0.53	1.35	0.36	2.7	6.4		

*For three representative training scans, one from each AD, SZ, and BI data sets, the parameters t_{min}, t_{max}, t_{grad}, p, and g were varied to minimize the segmentation error E. The column E_{opt} lists the minimum error achieved. E_{med} is the error that results from the use of the median value of of *Bridge Burner* parameters across the three training cases.

Measures of Accuracy and Agreement

Among measures used to assess segmentation accuracy and interobserver agreement, the simplest is the volumetric overlap of the brain masks considered as sets. If A is a mask constructed by the segmentation algorithm and G the ground truth mask, we can compute the relative oversegmentation error OSE as $v(A \backslash G)/v(G)$, where the symbol \ denotes the set difference and v is the volume or the number of voxels in the set. Similarly, the relative undersegmentation error USE is computed as $v(G \backslash A)/v(G)$. The overall segmentation error E is:

$$E = \frac{v(A \backslash G) + v(G \backslash A)}{v(G)}. \quad [7]$$

$E = 0$ implies perfect accuracy, i.e., full volumetric agreement with the ground truth. When comparing masks A and B generated by two experts, the interobserver agreement was measured as:

$$E' = \frac{v(A \backslash B) + v(B \backslash A)}{0.5 \cdot (v(A) + v(B))}. \quad [8]$$

Another commonly used measure of segmentation error is the distance between their surfaces. We computed such measure as:

$$H(A,B) = \frac{1}{n_A} \sum_{a \in surf(A)} dist(a,B) + \frac{1}{n_B} \sum_{b \in surf(B)} dist(b,A) \quad [9]$$

where surf(A) is the set of surface voxels of A, n_A is the number of voxels in S(A), and dist(x,Y) is the Euclidean distance between a voxel x and the nearest surface voxel of Y. Since every fifth section was used in the analysis, the distance was approximated by a two-dimensional (in-plane) computation.

Optimization of Bridge Burner and BET Parameters

After evaluating interobserver agreement, three MRI scans (one each from BI, AD, and SZ data sets) were selected and used to optimize the five parameters of *Bridge Burner* (t_{min}, t_{max}, t_{grad}, p, g) and the two parameters of BET (b_t, t_{CSF}). Selected were the scans with median value of interobserver agreement E', as these were deemed to be most representative. For each of the three cases the parameters were varied to minimize the

overall segmentation error E. Due to a limited number ($N = 3$) of 512×512 cases used, we did not include any high-resolution MRI in the optimization procedure.

RESULTS

A visual inspection of all test images confirmed the correct placement of the $1 \times 1 \times 1$-cm^3 seed box entirely within the white matter.
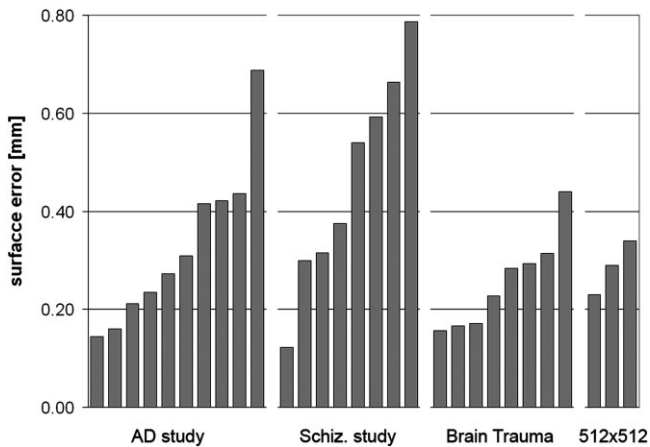
The optimal parameters for three representative scans and corresponding segmentation errors E_{opt} are shown in Table 1. When segmentations were recomputed using the median values of these parameters, the accuracy remained virtually unchanged (column E_{med} in Table 1), suggesting that the method tolerates well suboptimal parameter values. In view of this finding, all 26 standard resolution cases were segmented with a single common set of *Bridge Burner* parameters $t_{min} = 0.53$, $t_{max} = 1.35$, $t_{grad} = 0.36$, $p = 2.7$, and $g = 6.4$. For the three high-resolution cases we used the same threshold parameters but doubled the value of p to 5.4 and g to 12.8.

Bridge Burner segmentation of one MRI dataset on a personal computer with Intel Pentium-4 3-GHz processor required approximately seven seconds, including five seconds for the 3D edge detection task.

Bridge Burner segmentation error E averaged 3.4% ± 1.3% of the brain volume (Fig. 3). While the average OSE (1.9%) was larger than USE (1.5%), the difference
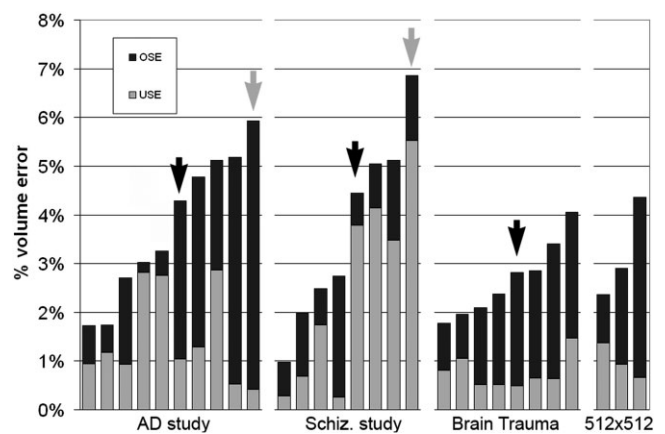
Figure 3. The plot of *Bridge Burner* oversegmentation (OSE) and undersegmentation error (USE) for 29 cases and four groups. Three representative cases (black arrows) are shown in Fig. 5. Two outliers (gray arrows) are shown in Figs. 6 and 7.
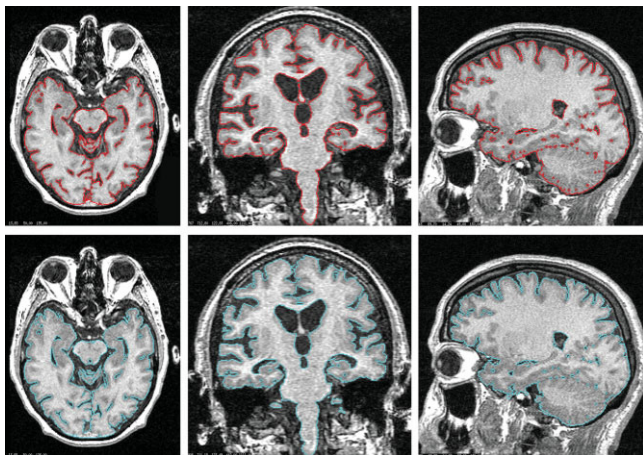
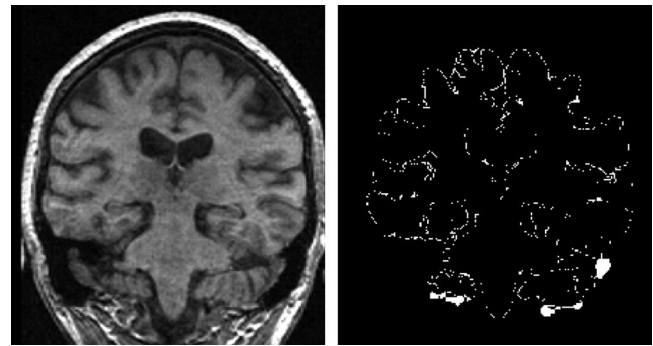**Figure 4.** The distribution of *Bridge Burner* surface errors.

Figure 6. The image (left panel) with the largest oversegmentation error. The right panel shows voxels falsely classified by *Bridge Burner* as the brain. Oversegmented voxels include a thin layer on the cortical surface, a large transverse sinus, and the meninges under the cerebellum.

between OSE and USE was not statistically significant because of their large variability across cases (Fig.3). The average surface error was 0.34 ± 0.17 mm (Fig. 4). Figures 5–7 illustrate representative results and the outliers. The optical nerves, facial muscle, scalp, and skull were successfully isolated from each brain.

The interobserver agreement E' among the corresponding brain masks generated manually by expert observers was $3.8\% \pm 2.0\%$. Interobserver agreement expressed in terms of surface distance was 0.48 ± 0.49 mm.

For BET program optimized on the same three training cases, after removal of CSF the segmentation errors E averaged $8.3\% \pm 9.1\%$. In four cases OSE was larger than 10%, with some facial features included in the brain mask. After excluding these four cases, BET segmentation error was reduced to $5.5\% \pm 2.1\%$, but even then BET accuracy was lower than for *Bridge Burner* (paired *t*-test, t = 6.71, df = 21, $P < 10^{-7}$). The largest positive difference between BET and *Bridge Burner* segmentation errors occurred in cases with visible signal

intensity nonuniformities, head motion, and increased slice thickness.

Scan-rescan differences (mean absolute difference normalized to the brain volume) of *Bridge Burner* volumes measured in the same individual at two different exams ranged 0.52% to 3.41% (average volume difference = 2.18%). When comparing volumes of two scans acquired in the same exam, without repositioning of the subject, the differences ranged 0.32% to 0.92%, with an average of 0.50%.
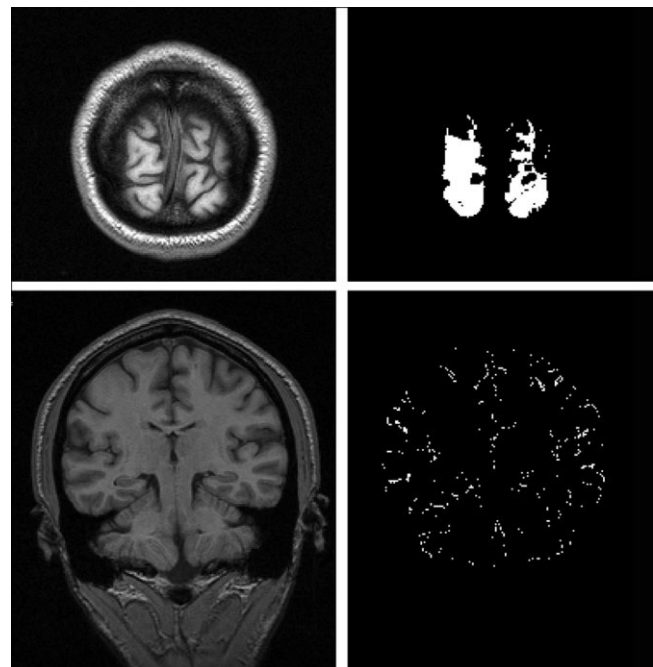

Figure 5. Three representative cases indicated by the black arrows in Fig. 3. Each case occupies one column. Top row (in red) the brain outline as segmented by the consensus of human experts. Bottom row (in blue): the outline of the brain masks segmented by *Bridge Burner*.

Figure 7. Left column: two slices from the image with the largest undersegmentation error. The right column depicts brain voxels that were not in *Bridge Burner* output. Most of the undersegmented voxels lie in the occipital lobe (upper row), where brain signal was approximately 50% brighter than in the central slices (lower row).
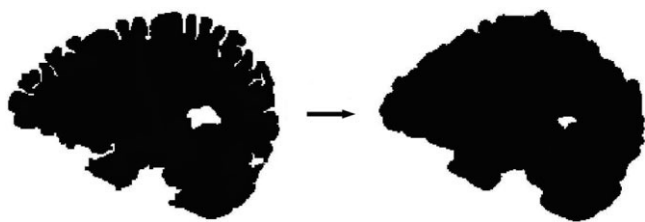
Figure 8. Left panel: a sagittal slice through the brain segmented by human experts. Right panel: simplifications introduced when a 3D morphological peel ($p = 2.7$) is followed by the conventional, unconstrained 3D growth ($g = 2.7$).

DISCUSSION

We described *Bridge Burner*, a method developed for automated brain segmentation from T1-weighted MRI. Because of our research interests in brain morphology, measurement of atrophy, and the need to coregister MRI and functional images, the algorithm was applied to relatively high-resolution ($256 \times 256 \times \sim100$), research quality MR images. When tested on a spectrum of such images, we achieved good $3.4\% \pm 1.3\%$ segmentation accuracy combined with processing speed of the order of five seconds.

With several important differences, *Bridge Burner* follows the "thresholding-with-morphology" approach (11,19–21). Variants of this approach have in the past been implemented in our laboratory, but their performance was not consistent, often requiring hand-editing to achieve acceptable results. Conventional implementations use unconstrained growth, integer values of the peel parameter p, and set $g = p$, thus introducing errors due to smoothing of brain contours (Fig. 8). It appears that increased reliability of *Bridge Burner* over conventional "thresholding-with-morphology" is due to our use of: 1) fractional values of p and g parameters and 2) constrained growth procedure.

In the majority of the cases, *Bridge Burner* brain masks are visually similar to the masks generated by the consensus of expert observers (Fig. 3). It is interesting to note that the interobserver discrepancy was larger than the average difference between *Bridge Burner* and the consensus of experts (3.8% vs. 3.4%). In spite of the fact that all datasets were T1-weighted images with similar contrast and signal to noise ratio, we have observed a wide (1–7%) range of accuracy across the cases. Meninges and large sinuses were the nonbrain structures most often falsely segmented as the brain.

Based on our scan-rescan results, the precision of volumetric estimates obtained from a serial 256×256 MRI using *Bridge Burner* is of the order of 2%. This level of precision is insufficient for detecting and monitoring subtle brain changes that may occur in neurodegenerating diseases. To analyze longitudinal data, more sophisticated algorithms based on partial volume detection and image coregistration may be required (22,23).

While we did not compare *Bridge Burner* with several recently reported brain segmentation algorithms (13,14,24), we found significantly lower brain segmentation error than BET, a computationally efficient and

widely used package. After excluding four failed cases and three high-resolution cases, BET error averaged 5.5%. This is similar to the 5.9% mean segmentation error of BET recently observed in segmenting images of healthy young volunteers (12). The comparison also suggested that the *Bridge Burner* algorithm is more robust than BET with respect to signal intensity non-uniformity and motion artifacts.

Our study resulted in a large database of 29 high-precision brain masks that represent the consensus of several human experts in neuroanatomy. This laborious effort required many months of manual tracings by multiple observers. Resulting brain masks could provide an important standardized resource for optimizing brain segmentation algorithms.

In conclusion, we have validated the *Bridge Burner* algorithm that segments the brain as the single, large, connected body devoid of thin and long features. *Bridge Burner* shows the desirable combination of accuracy, efficiency, and robustness. While we recognize that for most applications accuracy is the key concern, the current trend of acquiring structural images at a resolution approaching 512^3 makes fast processing speed an important attribute of this algorithm. Since there is no attempt to model the brain, or to take advantage of a priori information about its size or shape, we expect the algorithm to be of use in segmenting other organs from MRI, CT, PET, and SPECT data.

REFERENCES

1. Frank RA, Galasko D, Hampel H, et al. Biological markers for therapeutic trials in Alzheimer's disease: NIA initiative on neuroimaging in Alzheimer's disease. Neurobiol Aging 2003;24:521–536.
2. Gunter JL, Shiung MM, Manduca A, Jack CR, Jr. Methodological considerations for measuring rates of brain atrophy. J Magn Reson Imaging 2003;18:16–24.
3. Fox NC, Schott JM. Imaging cerebral atrophy: normal ageing to Alzheimer's disease. Lancet 2004;363:392–394.
4. Thompson PM, MacDonald D, Mega MS, Holmes CJ, Evans AC, Toga AW. Detection and mapping of abnormal brain structure with a probabilistic atlas of cortical surfaces. J Comput Assist Tomogr 1998;21:567–581.
5. Ashburner J, Csernansky JG, Davatzikos C, Fox NC, Frisoni GB, Thompson PM. Computer-assisted imaging to assess brain structure in healthy and diseased brains. Lancet Neurol 2003;2:79–88.
6. Shen D, Davatzikos C. Very high resolution morphometry using mass-preserving deformations and HAMMER elastic registration. Neuroimage 2003;18:28–41.
7. Bookstein FL. Endophrenology: new statistical techniques for studies of brain form. Life on the hyphen in neuro-informatics. Neuroimage 1996;4:S36–S38.
8. Woods RP, Cherry SR, Mazziotta JC. Rapid automated algorithm for aligning and reslicing PET images. J Comput Assist Tomogr 1992; 16:620–633.
9. Studholme C, Hill DL, Hawkes DJ. Automated three-dimensional registration of magnetic resonance and positron emission tomography brain images by multiresolution optimization of voxel similarity measures. Med Phys 1997;24:25–35.
10. Smith SM. Fast robust automated brain extraction. Hum Brain Mapp 2002;17:143–155.
11. Shattuck DW, Leahy RM. Brain Suite: a cortical surface identification tool. Med Image Anal 2002;6:129–142.
12. Boesen K, Rehm K, Schaper K, et al. Quantitative comparison of four brain extraction algorithms. Neuroimage 2004;22: 1255–1261.

13. Segonne F, Dale AM, Busa E, et al. A hybrid approach to the skull stripping problem in MRI. Neuroimage 2004;22:1060–1075.

14. Fennema-Notestine C, Ozyurt IB, Clark CP, et al. Quantitative evaluation of automated skull-stripping methods applied to contemporary and legacy images: effects of diagnosis, bias correction, and slice location. Hum Brain Mapp 2006;27:99–113.

15. Monga O, Deriche R, Malandain G, Cocquerez J. Recursive filtering and edge tracking: two primary tools for 3-D edge detection. Image and Vision Computing 1991;4:203–214.

16. Tsui WH, Rusinek H, Van Gelder P, Lebedev S. Analyzing multimodality tomographic images and associated regions of interest with MIDAS. SPIE Medical Imaging: Image Processing 2001;4322: 1725–1734.

17. Duvernoy HM. The human brain: surface, three-dimensional sectional anatomy and MRI. New York: Springer-Verlag, 1991. 554 p.

18. Warfield SK, Zou KH, Wells WM. Simultaneous truth and performance level estimation (STAPLE): an algorithm for the validation of image segmentation. IEEE Trans Med Imaging 2004;23:903–921.

19. Höhne K, Hanson W. Interactive 3D segmentation of MRI and CT volumes using morphological operations. J Comput Assist Tomogr 1992;16:185–294.

20. Bomans M, Höhne KH, Tiede U, Riemer M. 3-D Segmentation of MR images of the head for 3-D display. IEEE Trans Med Imaging 1990; 9:77–183.

21. Goutsias J, Vincent L, Bloomberg DS. Mathematical morphology and its applications to image and signal processing. Boston: Kluwer Academic Publishers; 2000. 445 p.

22. Rusinek H, De Santi S, Frid D, et al. Regional brain atrophy rate predicts future cognitive decline: 6-year longitudinal study of normal aging. Radiology 2003;229:691–696.

23. Rusinek H, Endo Y, De Santi S, et al. Atrophy rate in medial temporal lobe during progression of Alzheimer disease. Neurology 2004;63:2354–2359.

24. Lee JM, Yoon U, Nam SH, Kim JH, Kim IY, Kim SI. Evaluation of automated and semi-automated skull-stripping algorithms using similarity index and segmentation error. Comput Biol Med 2003; 33:495–507.